Journal of Power Sources xxx (2017) xxx-xxx

Contents lists available at ScienceDirect

Journal of Power Sources

journal homepage: www.elsevier.com

Carbonate scale deactivating the biocathode in a microbial fuel cell

M. Santini [a, 1], S. Marzorati [b, 1], S. Fest-Santini [c], S. Trasatti [b], P. Cristiani [d, *]

[a] Department of Engineering and Applied Sciences, University of Bergamo, Dalmine, Italy
[b] Dipartimento di Chimica, Università degli Studi di Milano, Milano, Italy
[c] Department of Management, Information and Production Engineering, University of Bergamo, Dalmine, Italy
[d] Ricerca sul Sistema Energetico – RSE SpA, Milano, Italy

ARTICLE INFO

Article history:
Received 7 December 2016
Received in revised form 26 February 2017
Accepted 27 February 2017
Available online xxx

Keywords:
3D MicroCT
Microbial fuel cells
Biocathode
Carbonate deposition
Scaling

ABSTRACT

The development and the following inactivation of a carbon-based biocathode in single chamber and membraneless MFCs was investigated in this work.

The electrochemical behavior of the biocathode has been analyzed over time during the MFC life. X-Ray Micro-Computed Tomographies (microCTs) have been carried out at progressive stages, documenting the building over time of a layer of scale deposition becoming thicker and thicker up to the cathode inactivation. The technique provides cross-sectional (tomographic) grayscale images and 3D reconstruction of volumes. Lighter color indicates lower X-ray attenuation (*i.e.*, lower atomic density) thus allowing distinguishing biofilm from inorganic fouling on the basis of the average atomic number Z of each voxel (3D pixel). MicroCT was combined with Scanning Electron Microscopy (SEM) and Energy-Dispersive X-Ray Spectroscopy (EDX) in order to qualitatively recognize chemical species in each different layer of the cathode's section.

Results correlated the presence of biofilm and calcium carbonate deposits, prevalently in the inner part of the cathode, with the produced electric current over time. A specific microCT-related software quantified the time-dependent carbonate scale deposition, identifying a correlation between the decreasing performances of the device and the increasing quantity of scale deposition that penetrates the cathode cross section in time.

1. Introduction

Microbial fuel cells (MFCs) are a novelty in the Fuel Cell panorama and the challenge of their industrialization is attracting more and more effort in research. This is because the potentialities of bioelectrochemical technologies span over a wide range of practical applications such as micro-electrical power production [1–3], organic wastes treatment [4–6], bio-hydrogen production, CO_2 reduction, biosensors and electro-fermentation of new valuable products from wastes [7,8]. Nonetheless, several drawbacks in materials and design have still to be overcome in order to reach competitive performance with respect to other more recognized technologies. High internal resistance, low current, low power production and resilience are still challenges in the case of MFC systems, in spite of the recent progresses achieved [9–11].

In a microbial fuel cell, bacteria settle on the electrodes and catalyze the oxidation of biodegradable organics (fuel) dissolved in the anodic compartment. In simple systems such as single chamber and membraneless MFCs, a porous cathode is directly exposed to the air from one side and to the solution containing the organic fuel and the bacteria inoculum from the other side. Therefore, the same initial bacteria pool colonizing the anode also forms a biofilm layer at the cathode. Biofilm plugs the porosity of the cathode and consumes oxygen, impeding its diffusion through the anode. Nevertheless, cathodic biofilm allows ions diffusion, the biofilm being composed of water for more than 90%. In this way, biofilm can act as good electrolytic separator between the anodic and cathodic region of the MFC [12] instead of polymeric membrane. The biofilm also switches the chemical cathodic reaction in a biochemical reaction, as it contextually catalyzes the reduction of oxygen to water [13,14]. On the other hand, bacteria excrete extracellular polymeric substances (EPS) in the biofilm that form a massive slime in which inorganic precipitates, corrosion products and particulates are glue. Negative effects can be consequently induced, due to biofouling that increases the mass transfer resistance at anode and cathode, depending on the environment, the electrochemical operative condition and the substrate [15,16].

Biofouling issues usually strongly affect also MFC systems equipped with electrolytic polymeric membranes, blocking or slowing down the mass transport of chemical components through the membrane [17–19].

Previous works documented a thick layer of carbonate formed as a consequence of the alkalinity induced by the ORR on cathodes operated for long time in single chamber MFCs and completely inactive [20]. The formation of the thick carbonate scale was supposed to be responsible for the MFC inactivation, but it was not possible to clearly document this assumption, as a thick layer of biofilm was also contextually documented other than the inorganic scale. Furthermore, the high level of PTFE used (higher than 60%) to make waterproof

* Corresponding author.
Email address: pierangela.cristiani@rse-web.it (P. Cristiani)
[1] The authors have contributed equally to the manuscript.

http://dx.doi.org/10.1016/j.jpowsour.2017.02.088
0378-7753/

the porous air cathode of the MFC was also found to inhibit the oxygen reduction reaction (ORR) [21]. To definitely clarify the cause the inactivation phenomenon on biocathode, the modification of a carbon cathode structure, in terms of electrochemical parameters, biofilm growth and scale formation, has been investigated in this work. Three different operating stages of single chamber and membraneless MFCs were investigated, during two months, with the aim of clearly differentiating and underlining the phenomenon of carbonate precipitation and the role of biofilm in the activation/decline of MFC performance. An inoculum of swine manure, typically rich in carbonates, and a carbonate buffered solution have been chosen in order to minimize the influence of a pH change in the anolyte and to accelerate the phenomenon of carbonates deposition.

The cathode morphology evolution was analysed by 3-dimensional X-ray Micro-Computed Tomography (3D microCT) technique, digitalizing 3D samples of wet carbon cathode with different operating times.

Cathode sample composition was analysed also with the Scanning Electron Microscopy technique and with the X-Ray microprobe for the analyses of the elements. The best performing stage and the subsequent deactivation of the electrochemical process have been documented.

2. Materials and methods

2.1. MFC setup

Three single chamber and membraneless MFCs as described in Ref. [13] were operated in batch configuration, respectively for 15, 30 and 60 days at 30 °C.

Swine manure was used as inoculum in the MFC. The inoculum was diluted in 1:10 in carbonate buffer (pH 7.8) and the COD measured was 1023 mg L^{-1}. Sodium acetate (Sigma-Aldrich) was periodically added during the experiment as fuel for bacterial metabolism (dosage of 3 g L^{-1} each acetate addition).

Cathodes were built from a square (3 × 3 cm) carbon cloth (SAATI C1) fortified with carbon powder following the optimized procedure described in Ref. [22]. The geometrical surface area exposed to the solution was a circle with 2 cm diameter. Anodes were made of the same carbon cloth (SAATI C1) without any addition of carbon powder, rolling a piece of 5 × 5 cm around an electrical connection with an insulated copper cable in a sort of cylinder occupying large part of the bottom of the anodic chamber [23]. The anode and cathode of the MFC were connected with an external load of 100 Ω. After operation, the cathodes were removed from the MFC, photographed and then cut in small pieces (10 × 15 mm) for SEM and 3D X-Ray microCT analyses.

2.2. Electrochemical measurements

The potential difference across the 100 Ω resistance (R) was acquired every 20 min with a multichannel Data Logger (Graphtech midi Logger GL820). The generated current (I) was calculated by the equation $I = V R^{-1}$, where I is the current flowing through the external resistance.

Power curves were performed on MFCs from open circuit voltage (o.c.p.) to short circuit using a Compactstat IVIUM potentiostat connected to a personal computer at a scan rate of 10 mV min^{-1}.

Linear sweep voltammetry was performed on cathodes. Experiments were performed with a classical three-electrodes configuration, using the Compactstat IVIUM potentiostat connected to a personal computer. Cathodes were used as working electrode, a platinum wire as counter electrode and an Ag/AgCl (KCl sat.) electrode as reference. A Luggin capillary was adopted to minimize the ohmic drop into the solution. Before each experiment, MFCs were allowed to equilibrate at their o.c.p. for at least 1 h. Potential was then moved at a scan rate of 10 mV min^{-1} from the o.c.p. to −0.5 V for polarization on cathodes. All the potentials throughout the text are referred to the Ag/AgCl (KCl sat.) reference electrode.

2.3. Chemical oxygen demand analysis

The soluble Chemical Oxygen Demand (sCOD) was periodically measured by a spectrophotometric method. A portion of solution sampled from each SMFC was centrifuged for 15 min at 6000 rpm, carefully added to HT-COD cuvette test (Hach Lange Gmbh), and digested at 175 °C for 15 min (Lange HT 200 S). Upon cooling, the COD value was read by an UV— spectrophotometer (Lange DR 3900).

2.4. SEM, EDS analyses

Microscopy observations (high vacuum Scanning Electron Microscope (SEM)-Field Emission Gun (FEG) mod. Mira II TESCAN) and analyses by the X-Ray microprobe (EDX) were performed on samples of cathodes (dried and coated by Au).

2.5. 3D tomographic technique

To determine fouling rates, 3D microCT technique was applied, and digitalized 3D objects of wet carbon cathode samples with different operating times were generated. To avoid undesired drying shrinkage during the X-ray acquisition, the cathode samples were inserted into sealed polypropylene PCR tubes. Such approach was already successfully applied in a previous work documenting the final stage of the carbonate scale formation [20]. The used microCT is based on an open type X-ray source 160 kV_p @ 200 μA, a flat panel CMOS detector and a high-precision air-bearing rotating stage. The objects to be investigated were placed on the stage and rotated by small angular steps. 2D radiographies were acquired at each rotation step. The number of radiographic projections is usually of several hundred and depends on the desired resolution as well as the dimension of the object. These projections were collected for a complete rotation (360°) and reconstructed using standard filtered back-projection algorithms. Here, the volume reconstruction is computed by the commercial software VGStudio MAX®.

From the reconstructed volume, substances differing in their X-Ray attenuations can be segmented. If the energy range was proper chosen and filtered, each substance is characterized by a peak in the global volumetric intensity histogram (see Fig. 1). In the presented grayscale of Fig. 1, lighter colors indicate higher X-ray attenuation, i.e. higher atomic density. The midpoint between adjacent peaks was chosen as separating value. Biofilm and electrode texture were composed both of carbons, although in different concentration, and could not be distinguished considering only their atomic number.

3. Results and discussion

3.1. MFCs performance

The voltage trends of the three testing MFCs measured across a resistance of 100 Ω during five cycle of acetate dosage are reported in Fig. 2. The MFC 1 operation was stopped after 15 days, when it reached the second peak (after the second acetate dosage). MFC 2 was stopped after 30 days, on a plateau of maximum power reached at fourth acetated dosage; MFC 3 was disconnected after 60 days and

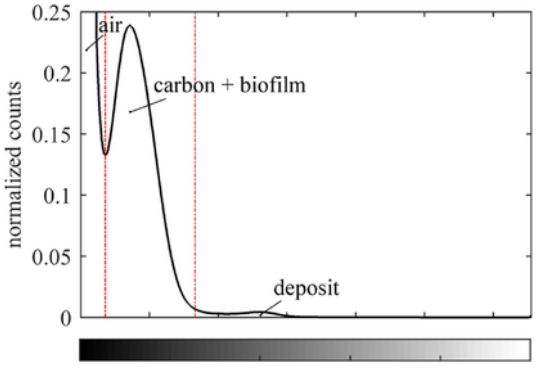

Fig. 1. Global intensity histogram of a reconstructed microCT volume (sample cathode operated 15 days); the red dashed lines indicate the thresholds between adjacent materials. (For interpretation of the references to colour in this figure legend, the reader is referred to the web version of this article.)

five feeding cycles, when the voltage increase was not more able to reach the previous high values, showing a clear loss of the performance.

The operating MFCs reached a maximum of almost 0.1 V during the first month and four dosages. This results is in agreement of previous test performed with the same system [13,22]. In fact, the single chamber MFCs generally reach a maximum peak of power in one month, followed by a more or less fast decline that depends on several parameters, including the pH variation out of the range between 5 and 9 [23] affecting the bacteria metabolism. The graphic of pH trend in the three operative MFCs is shown in Fig. 1. It indicates that the carbonate buffer power of the solution was able to control the pH in a range favorable for the microorganisms growth during all the experimentation. No significant alkalization, nor acidification of the solution occurred. In the MFC operated for longer time, a sharp decrease of pH prevailed.

Two power curves of MFC 2are shown in Fig. 3. The first curve was performed just after the second voltage peak, detecting a maximum power density of about 1.6 W m^{-2}. The second curve was performed two day after, at the end of the second feeding cycle, when the lack of fuel (under 200 mg L^{-1} COD) caused the voltage density fall. The presence of an overshoot in this curve is visible. This phenomenon is frequent in under-performing MFC systems, where the internal resistance is high [24,25] and it could be explained in this case with a not sustained oxidizing reaction rate on the anode.

The polarization curve performed on the cathodes of MFC 2 at different level of voltage is shown in Fig. 4. They indicate that the cathode is able to sustain a sufficient current for the global process also when acetate is consumed by bacteria during the first three feeding cycles. On the contrary, the polarization curve performed after 60 days (on a not more operating MFC) evidences how the cathodic reaction is completely inhibited at this stage. In fact, the frame detailed in the graphic shows that the current stimulated from the polarization was three order of magnitude lower (μA) than that (mA) achieved in the previous stages.

3.2. 3D and 2D morphological analyses of cathodes

A picture of the water-side surface of the cathodes operated respectively for 15, 30 and 60 days is reported in Fig. 5.

The biofilm is clearly visible on the surface of the cathode in the photos (a), (b), and (c), although in (c) it was removed together with the carbonate and carbon MPL to some extent before taking the picture.

The visual inspection of the MFC cathode confirmed the presence of a thick biofilm facing the anodic compartment and a white precipitate beneath biofilm after 60 days operated cathode. Soluble (sodium carbonate) deposit was also visible in the external face air side, as previously documented [13,20]. By washing the external face of the cathode, the soluble sodium carbonate was completely removed before the analyses at SEM and at 3D-Tomography.

3D renders of the cathode samples are shown in Fig. 5. The microCT volumes of the cathode samples were processed to differentiate carbon electrode texture and biofilm from scaling phenomena. The scaling of carbonate deposit was colored in blue as to be distinctly visible from the carbon layers and biofilm. The cathode facing the solution is the upper part of the renders. The air side cathode is not visible being on the bottom part. Part of the render of each sample reproduces just the layer of carbonates excluding biofilm and carbon for the half. The carbon particles forming a microporous thick layer on the carbon cloth cathode, water side, is the remaining dark part, well visible in the three photos of Fig. 5. These particles are well evidenced in the 3D renderings, being the black and massive part of the thickness. The carbon cloth texture is better visible on the uncovered areas of the samples in the photos. It is just discernable at the bottom of the thickness in the renders, being made of the same material of the microporous carbon particles.

The 3D-renders (a) show granular carbonates early enucleating after just 15 days of cathode operating. Carbonate deposition is more pronounced on the wet side of the cathode than on the air side. Carbonates precipitation is evidenced in the area where spots of growing biofilm was detected, on the wet surface of the cathode.

Biofilm is not clearly visible in the 3D render (a) after 15 days operating in MFC, but it is clearly visible as a uniform layer on the top part of rendered surfaces, covering the carbonate deposits after 30 and 60 days operating period.

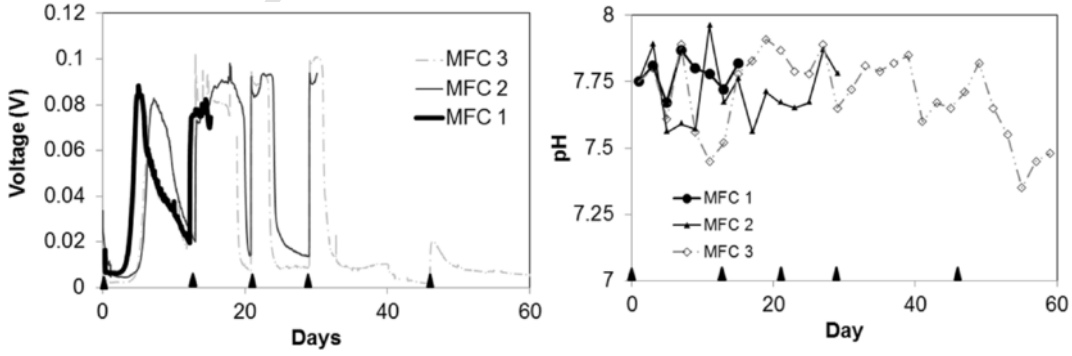

Fig. 2. Trends of voltage and pH in the MFC operated respectively for 15, 30 and 60 days. The black tringles indicate a new acetate dose.

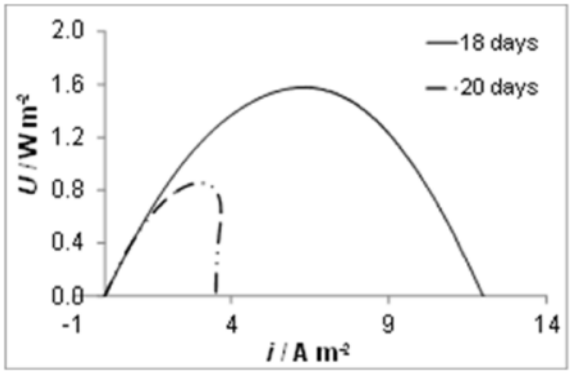

Fig. 3. Power density curve recorded on the second peak and at the end of it in MFC 2 (day 18 and 20 respectively).

After 30 days, a completely developed layer of biofilm appears on the surface, whose thickness decreases after 60 days, over a compact layer of inorganic deposits. At this stage, carbonates form a uniform "wall" beneath biofilm. Small isolated particles of carbonate scaling are visible inside the carbon layer and a more consistent scale encrusts the fibers of the carbon cloth. The shape of fibers of carbon cloth is underlined from the scaling phenomenon in the layer on the bottom of the render (c).

Cross-sections of the cathodes operated (a) 15 days, (b) 30 days and (c) 60 days respectively are shown in Fig. 6. SEM micrographs are reported on the top of the figure and 2D MicroCT slices are reproduced on the bottom of the figure.

The SEM micrographs well evidence the carbon cloth fibers, although their position in the sections is not completely authentic but, especially in (b), frayed and crushed, due to the cut and the sample arrangement before the analyses. In these images it is difficult to clearly distinguish carbonates from carbon matter and biofilm. On the other hand, carbonates are well evidenced in yellow in the 2D MicroCT slices. The carbon cloth texture is also evidenced in the slices, being the grey shadows just under the red line that signs the external surface of the cathode. The biofilm is the soft layer covering the section at the top, evidenced in yellow.

The 2D and 3D renders of cathode sections in Figs. 6 and 7 clearly show the progression of inorganic deposits beneath the biofilm and internally in the carbon cathode thickness, where the water infiltrates following preferential routes. The electrochemical performance followed the feeding cycles (Figs. 2 and 3) when biofilm developed on the electrodes.

The biofilm, initially patchy growing on the cathode wet side, reaches a maximum thickness at 30 days operating cathode (Figs. 5 and 6), then decreases in thickness at 60 days.

A thick biofilm on the cathode visible after 30 days is associated to a well performing cathode (Fig. 4), when MFC was at the maximum of the voltage (Fig. 2).

Carbonate particles are evidenced in the region of the cathode where biofilm was detected or could form as consequence of water leaching. The most thick deposits of carbonates are detected after 60 days, when MFC stopped working in consequence of the cathode inactivation, as clearly shown with the polarization curves of Fig. 4.

These results are in agreement with previous experimentation [20] and evidence the strict correlation of solid deposits enucleation with the electroactivity of living biofilm on the cathode.

3.3. Quantitative estimation of carbonates from 3D tomographic data

MicroCT volumes were also analyzed to gain quantitative information about the carbonate precipitation onto cathode surface areas for the three considered operation times. Digitalized volumes are of voxelized nature, and any feature to be extracted is jagged. This step size corresponds exactly to the size of one voxel. Such problem cannot even be solved by smoothing the extracted surfaces, as the gain in terms of reduction of spurious steps is counterbalanced by the reduction in the accuracy of tracking of the real contour [24].

These problems of contour measurements, particularly for 2D applications, are well known. Here, the algorithm proposed by Vossepoel et al. [25] was applied on slice basis. Firstly, the cathode surface line was expressed by means of a starting point and a chain code [26], where all the pixels on the contour are memorized as numbers. Even numbers indicate straight vertical or horizontal motion and odd values diagonal motions. Number of changes between consecutive values in the chain code was considered in the addend "corners". The length of the real contour of the cathode surface is then calculated as:

$$L_{real} = 0.980 \cdot N_{even} + 1.406 \cdot N_{odd} + 0.091 \cdot N_{corner} \quad (1)$$

and visualized in red in Fig. 6. The same approach was used to estimate circumferences of the precipitation. In a second step, their surface were calculated.

These areas are rendered light blue in Fig. 6. The deposit volume (V) to cathode surface (S) ratio was than calculated assuming 1 voxel

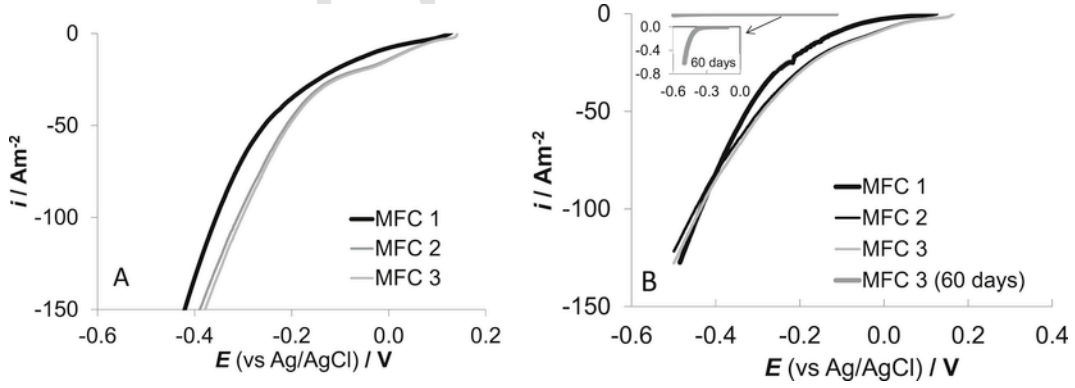

Fig. 4. Polarization curves (cathode) recorded on the voltage peak of the first acetate cycle (A), at the end of the third cycle (B) and after 60 days of operating MFCs (magnified in the frame).

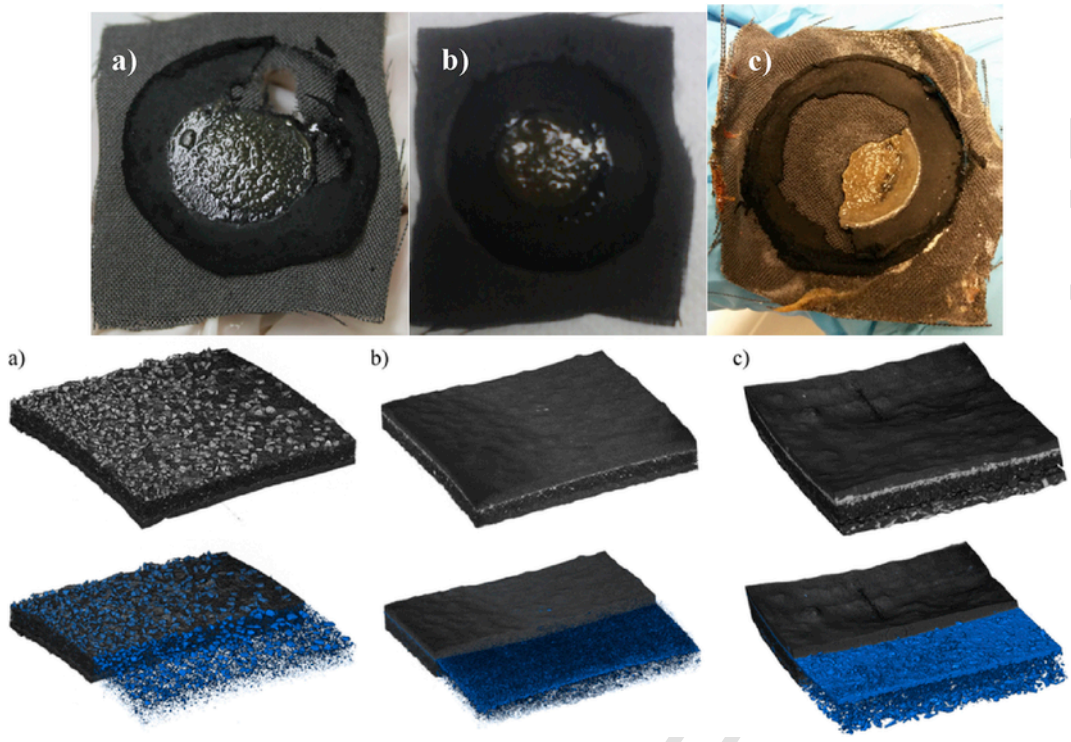

Fig. 5. Photographs and 3D MicroCT renders of cathode surface operated (a) 15 days, (b) 30 days and (c) 60 days respectively. The carbonates growth is underlined and colored in blue in the renders at the bottom, without carbon layer and biofilm layers for half part. (For interpretation of the references to colour in this figure legend, the reader is referred to the web version of this article.)

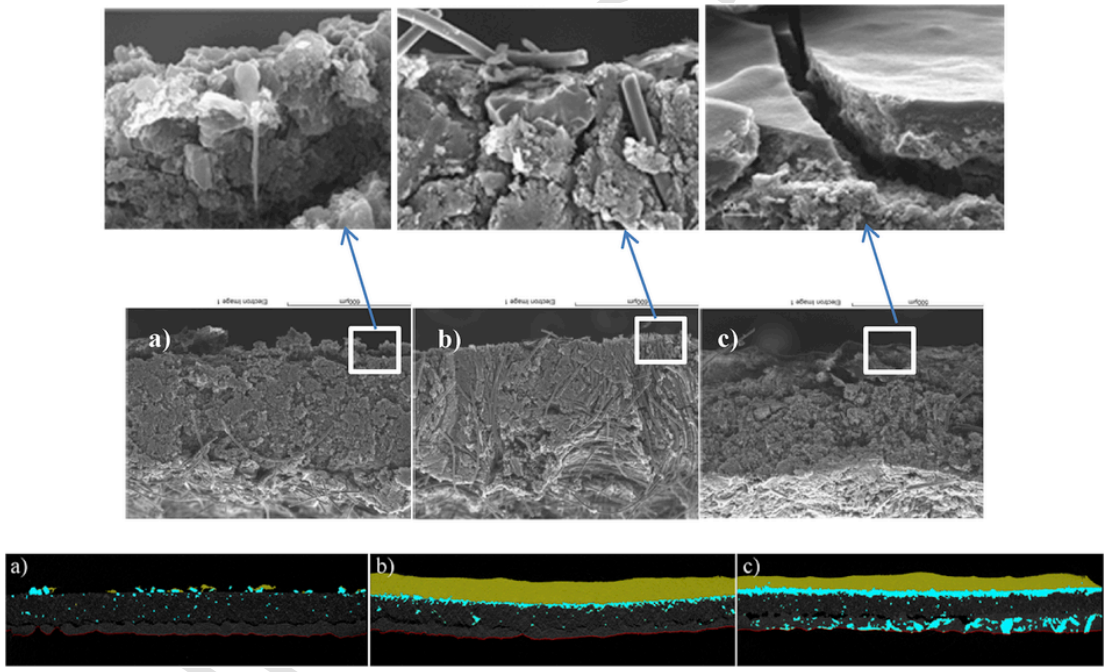

Fig. 6. SEM micrographs and 2D MicroCT (slices) of cross-sections of cathode samples operated (a) 15 days, (b) 30 days and (c) respectively. Biofilm (yellow), carbonate deposits (light blue) and the external surface line (red) is rendered in the 2D MicroCTs. (For interpretation of the references to colour in this figure legend, the reader is referred to the web version of this article.)

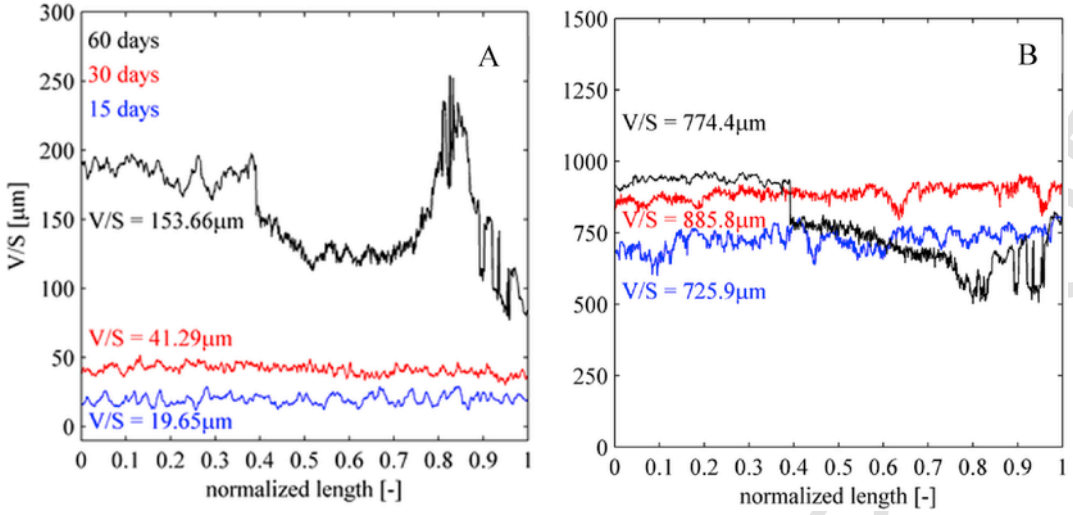

Fig. 7. Thickness (V/S) of scale deposition per unit area of the 3D renders of the cathodes samples (A); Total thickness per unit area of the 3D renders of the biofouled cathodes samples operated for 15, 30 and 60 days respectively (B).

width for both:

$$\frac{V}{S} = \frac{\sum_{i=1}^{N} S_{deposit,\,i}}{\sum_{i=1}^{N} L_{real,\,i}} \qquad (2)$$

The volume to surface ratio for each single slice and the overall value obtained with equation (2) is shown in the graphics of Fig. 7. The cathode sample operated 60 days features a relevant but non-uniform distribution of carbonate per unit surface.

The same approach was used to calculate the volume to surface ratio for each single slice and the overall value obtained with equation (2) for the carbon layer plus biofilm. The results are reported in Fig. 7. The trend of the total thickness of the cathodes, including biofilm, and the sole carbonates *vs* the exposition time and *vs* the integrated charge produced by the three MFCs, are reported in Fig. 8.

3.4. Chemical equilibria influence to the salt precipitation

The elementary analyses performed on the transversal section of the sampled cathodes after 15 days operating stages (Fig. S1 Supporting information) evidenced Na and K enriched some regions on the external surface. This result indicates that water reached the external part of the cathode (air side). Ca enriched just the internal part of the cathode, at the interface with the solution beneath the biofilm.

The elementary analyses performed on the transversal section of the sampled cathodes at 30 days operating stages (Fig. S2 Supporting information), evidenced that Na and K uniformly imbibed the carbon particles of the microporous cathode, indicating the full and uniform penetration of water in the cathode section. Again, the most significant deposit of Ca are in the internal layer, with a clear progression from the internal to the external side of the cathode. Oxygen is evidenced mainly in the external layer, indicating that negligible oxygen was able to penetrate the cathode thickness forming oxides. Particles containing Si that were initially detected spread uniformly in the cathode section were enriched through the section, from the wet face through the air face of the cathode.

After 60 days, the elementary analyses of transversal section of the not more operating cathodes (Fig. S3 Supporting information) evidence an inhomogeneous distribution of elements, underlying the presence of cracks and preferential routes in the carbon layer that allowed the penetration and accumulation of water, biofilm and carbonates inside them. Mg is evidenced in the fissured area mostly like Ca, indicating the mixed nature of precipitates. Oxygen, as well as Si, K and Na is more evidenced in the external layer and in the cracks.

The pH in the solution does not increase over time (Fig. 2) and the temperature remained fixed at 30 °C during the test, in condition which does not favour the salts precipitation. The $CaCO_3$ solubility constant (k_{ps}) is $8.7 \cdot 10^{-9}$, is few orders of magnitude lower than the k_{ps} of $MgCO_3$ ($6.8 \cdot 10^{-6}$), but both of them are clearly far from the k_{ps} of Na_2CO_3 (1.2) of several orders of magnitude.

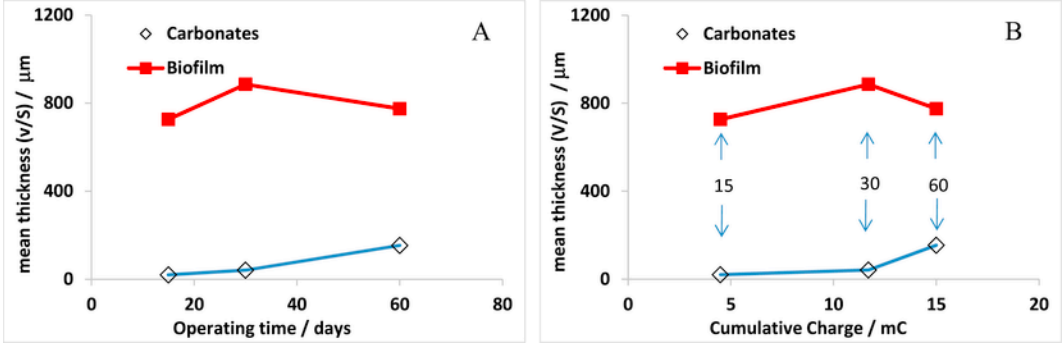

Fig. 8. Mean thickness of biofouled cathode samples *vs* operating time (A) and *vs* cumulative charge transferred (B).

From equation (3) it is possible to calculate the solubility (S) that increase as pH decrease (Fig. S4 supporting information).

$$S = \sqrt{k_{ps}\left(\frac{[H^+]^2}{k_{a1}k_{a2}} + \frac{[H^+]}{k_{a2}} + 1\right)} \quad (3)$$

In equation (3) the constant k_{a1} is $3.5 \cdot 10^{-7}$ and k_{a2} is $5 \cdot 10^{-11}$.

Since pH in the anodic (single) chamber remains close to the neutrality and at constant temperature, Ca and Mg carbonates can precipitate mainly in consequence of the local alcalinization of the solution in the surrounding of cathodic active sites, due to the oxygen reduction reaction (ORR) (4). It is possible to conclude, consequently, that on the cathode where neither deposits nor biofilm traces are evidenced, the cathodic reaction does not actively occurred.

$$O_2 + 2H_2O + 4\ e^- \rightarrow 4OH^- \quad (4)$$

Cracking and fessuration of the carbon layer were probably due to a mechanical stress induced by carbonate precipitation. This phenomenon allowed water and bacteria to reach and colonize the carbon cloth of the external surface through preferential routes. The deposits of carbonates on carbon cloth and preferential routes are evidenced in the 3D and 2D renders of Fig. 5 (c) and 6 (c). A significative ORR occurrence in other part of cathode than beneath the internal biofilm layer is documented with the formation of scale particles occluding the space between the carbon cloth fibers at the end of the tests.

The phenomenon of water leachage along preferential routes affected the fate of Si deposits that are present as impurity in the carbon particles of the cathode. In fact, Si enriched the surface of the cracks and the formed cavities of the carbon layer (Fig. S3).

Silicate forms from Si oxydes in alkaline solution in agreement with the reaction (5), but this deposits does not attach tightly to the carbon fiber as the Ca does and can, consequently, migrate with water. Indeed, the solubility of Na_2SiO_3 increases in presence of NaOH [24].

$$SiO_2 + 2NaOH \rightarrow Na_2SiO_3 + H_2O \quad (5)$$

Differently from Si, Ca shows a significant affinity to the carbon particles that impedes its draining away from the formation sites. In fact, the 3D renders of Fig. 5 evidence the process of thickening of the scale particles inside the cathode and beneath biofilm in particular.

The volume of deposited carbonates initially shows a direct correlation with the electric energy producted, in terms of coulombs. After 30 days, the charge transfer slows down and the carbonate deposition increases, highlighting a phenomenon of ion mass transport that becomes more important, accordly with the image of the growing "wall" shown comparing the 3D renders evolution. As a matter of fact, carbonate brick growth decreased strongly the microporosity of the cathode.

Comparing the graphics of Fig. 8, it is evident that the carbonates deposition increases strongly as the charge decreases. On the contrary, the biofilm decrease is coherent with the decrease of the charge. These results clearly evidence the predominant role of carbonate in decreasing the MFC performance up to the complete deactivation of the power. It is reasonable to infer that the "wall" of carbonates should have inhibited the bacteria growth in the biofilm, creating a barrier for the exchanging of nutrients and secreted metabolites between the air side of the cathode and the water side.

The high rate of carbonate scaling in this experiment mainly depends on the high concentration of bicarbonate buffering the solution. Bicarbonates equilibrium moves to carbonates when the pH rises over 10, close to the cathode due to the ORR.

Calcium carbonate generated from the acetate combustion (reaction 6) during MFC operation, calculated from cumulative charge (Fig. 8), was equal to 1, 3 and 3.9 mg after 15, 30 and 60 days, respectively. The gravimetric quantity of calcium carbonate estimated from the number of the voxel in the 3D renders is 16, 36 and 135 mg after 15, 30 and 60 days, respectively. If bicarbonate salts are not added in solution and MFC is operative with high coulombic efficiency, the contribute of fuel combustion (reactions 6–8 for sodium acetate) could be more relevant in the global balance of the carbonates deposited at the cathode, and the scaling process might be more or less fast over time.

$$CH_3COONa + 2O_2 \rightarrow 2CO_2 + Na^+ + OH^- + H_2O \quad (6)$$

$$CO_2 + Na^+ + OH^- \rightarrow HCO_3^- + Na^+ \quad (7)$$

$$HCO_3^- + Na^+ + OH^- \rightarrow CO_3^{2-} + Na^+ + H_2O \quad (8)$$

4. Conclusion

The modification of cathode structure, in terms of electrochemical parameters, biofilm growth and scale deposition has been studied in this work at three different operating stages of single chamber and membraneless MFC: i) when the MFC reached the maximum of power produced, ii) just before MFC declined the electric performance and iii) when the MFC resulted completely deactivated.

The results indicate that a local alkalinisation subsequent to the ORR beneath biofilm is the mechanism that, in feedback with the MFC power production, can cause the precipitation of carbonates. Cathodic sites are evidenced by the carbonate nucleation and growth. The renders of cathodes from the 2D- and 3D-microCT indicate that an effective ORR preferentially occurs in the region of the carbon electrode colonized by electro-active biofilm. The mechanism of biocathode in enhancing the ORR catalysis needs specific investigation and microbial analyses to be documented, nevertheless, the ORR inhibition due to carbonate was clearly evidenced by tomography. The carbonates particles grew thicker and thicker, becoming bricks of impermeable wall that fissures the cathode structure. This phenomenon allowed the water leakage on the air face, but impeded the mass transport of ions between electrode and biofilm up to the complete deactivation of the biocathode and the consequent deactivation of the global MFC process.

Acknowledgement

This work has been financed by the Research Fund for the Italian Electrical System (decree of March 19, 2009).

Many thanks to Dr. M. Lorenzi that performed the Micro-CTs and to Dr. Edoardo Guerrini that performed the SEM micrographs.

Appendix A. Supplementary data

Supplementary data related to this article can be found at http://dx.doi.org/10.1016/j.jpowsour.2017.02.088.

References

[1] F. Zhang, L. Tian, Z. He, Powering a wireless temperature sensor using sediment microbial fuel cells with vertical arrangement of electrodes, J. Power Sources 196 (2011) 9568–9573, http://dx.doi.org/10.1016/j.jpowsour.2011.07.037.

[2] A. Schievano, A. Colombo, M. Grattieri, S.P. Trasatti, A. Liberale, P. Tremolada, et al., Floating microbial fuel cells as energy harvesters for signal transmission from natural water bodies, J. Power Sources 340 (2017) 80–88, http://dx.doi.org/10.1016/j.jpowsour.2016.11.037.

[3] H. Wang, J.-D. Park, Z.J. Ren, Practical energy harvesting for microbial fuel cells: a review, Environ. Sci. Technol. 49 (2015) 3267–3277, http://dx.doi.org/10.1021/es5047765.

[4] X.A. Walter, A. Stinchcombe, J. Greenman, I. Ieropoulos, Urine transduction to usable energy: a modular MFC approach for smartphone and remote system charging, Appl. Energy (2016) http://dx.doi.org/10.1016/j.apenergy.2016.06.006.

[5] Gajda I, Greenman J, Melhuish C, Ieropoulos IA. Electricity and disinfectant production from wastewater: MFC Microbial Fuel Cell as self-powered electrolyser. Sci. Rep.. http://dx.doi.org/10.1038/srep25571.

[6] V.G. Gude, Wastewater treatment in microbial fuel cells – an overview, J. Clean. Prod. 122 (2016) 287–307, http://dx.doi.org/10.1016/j.jclepro.2016.02.022.

[7] A. Schievano, T. Pepé Sciarria, K. Vanbroekhoven, H. De Wever, S. Puig, S.J. Andersen, et al., Electro-fermentation - merging electrochemistry with fermentation in industrial applications, Trends Biotechnol. 34 (2016) 866–878, http://dx.doi.org/10.1016/j.tibtech.2016.04.007.

[8] K. Chandrasekhar, K. Amulya, S.V. Mohan, Solid phase bio-electrofermentation of food waste to harvest value-added products associated with waste remediation, Waste Manag. 45 (2015) 57–65, http://dx.doi.org/10.1016/j.wasman.2015.06.001.

[9] T.H.J.A. Sleutels, A. Ter Heijne, C.J.N. Buisman, H.V.M. Hamelers, Bioelectrochemical systems: an outlook for practical applications, ChemSusChem 5 (2012) 1012–1019, http://dx.doi.org/10.1002/cssc.201100732.

[10] P. Pandey, V.N. Shinde, R.L. Deopurkar, S.P. Kale, S.A. Patil, D. Pant, Recent advances in the use of different substrates in microbial fuel cells toward wastewater treatment and simultaneous energy recovery, Appl. Energy 168 (2016) 706–723, http://dx.doi.org/10.1016/j.apenergy.2016.01.056.

[11] S.B. Pasupuleti, S. Srikanth, S. Venkata Mohan, D. Pant, Continuous mode operation of microbial fuel cell (MFC) stack with dual gas diffusion cathode design for the treatment of dark fermentation effluent, Int. J. Hydrogen Energy 40 (2015) 12424–12435, http://dx.doi.org/10.1016/j.ijhydene.2015.07.049.

[12] E. Guerrini, M. Grattieri, S.P. Trasatti, M. Bestetti, P. Cristiani, Performance explorations of single chamber microbial fuel cells by using various microelectrodes applied to biocathodes, Int. J. Hydrogen Energy ().

[13] P. Cristiani, M.L. Carvalho, E. Guerrini, M. Daghio, C. Santoro, B. Li, Cathodic and anodic biofilms in single chamber microbial fuel cells, Bioelectrochemistry 92 (2013) 6–13, http://dx.doi.org/10.1016/j.bioelechem.2013.01.005.

[14] M. Daghio, I. Gandolfi, G. Bestetti, A. Franzetti, E. Guerrini, P. Cristiani, Anodic and cathodic microbial communities in single chamber microbial fuel cells, N. Biotechnol. 32 (2015) 79–84.

[15] G. Pasternak, J. Greenman, I. Ieropoulos, Regeneration of the power performance of cathodes affected by biofouling, Appl. Energy 173 (2016) 431–437, http://dx.doi.org/10.1016/j.apenergy.2016.04.009.

[16] E. Guerrini, P. Cristiani, M. Grattieri, C. Santoro, B. Li, S. Trasatti, Electrochemical behavior of stainless steel anodes in membraneless microbial fuel cells, J. Electrochem Soc. (2014) H62–H67, http://dx.doi.org/10.1149/2.096401jes.

[17] Y.-P. Wang, X.-W. Liu, W.-W. Li, F. Li, Y.-K. Wang, G.-P. Sheng, et al., A microbial fuel cell–membrane bioreactor integrated system for cost-effective wastewater treatment, Appl. Energy 98 (2012) 230–235, http://dx.doi.org/10.1016/j.apenergy.2012.03.029.

[18] A microbial fuel cell–membrane bioreactor integrated system for cost-effective wastewater treatment.pdf n.d. https://www.scribd.com/document/323075161/A-microbial-fuel-cell-membrane-bioreactor-integrated-system-for-cost-effective-wastewater- (Accessed 16 September 2016).

[19] S. Sevda, X. Dominguez-Benetton, K. Vanbroekhoven, H. De Wever, T.R. Sreekrishnan, D. Pant, High strength wastewater treatment accompanied by power generation using air cathode microbial fuel cell, Appl. Energy 105 (2013) 194–206, http://dx.doi.org/10.1016/j.apenergy.2012.12.037.

[20] M. Santini, M. Guilizzoni, M. Lorenzi, P. Atanassov, E. Marsili, S. Fest-Santini, et al., Three-dimensional X-ray microcomputed tomography of carbonates and biofilm on operated cathode in single chamber microbial fuel cell, Biointerphases 10 (2015) 31009, http://dx.doi.org/10.1116/1.4930239.

[21] E. Guerrini, M. Grattieri, A. Faggianelli, P. Cristiani, S. Trasatti, PTFE effect on the electrocatalysis of the oxygen reduction reaction in membraneless microbial fuel cells, Bioelectrochemistry 106 (2015) 240–247.

[22] C. Santoro, K. Artyushkova, S. Babanova, P. Atanassov, I. Ieropoulos, M. Grattieri, et al., Parameters characterization and optimization of activated carbon (AC) cathodes for microbial fuel cell application, Bioresour. Technol. 163 (2014) 54–63, http://dx.doi.org/10.1016/j.biortech.2014.03.091.

[23] E. Guerrini, P. Cristiani, S.P. Marcello Trasatti, Relation of anodic and cathodic performance to pH variations in membraneless microbial fuel cells, Int. J. Hydrogen Energy 38 (2013) 345–353.

[24] H.C. Boghani, J.R. Kim, R.M. Dinsdale, A.J. Guwy, G.C. Premier, Control of power sourced from a microbial fuel cell reduces its start-up time and increases bioelectrochemical activity, Bioresour. Technol. 140 (2013) 277–285, http://dx.doi.org/10.1016/j.biortech.2013.04.087.

[25] J. Winfield, I. Ieropoulos, J. Greenman, J. Dennis, The overshoot phenomenon as a function of internal resistance in microbial fuel cells, Bioelectrochemistry 81 (2011) 22–27, http://dx.doi.org/10.1016/j.bioelechem.2011.01.001.